Acetylcholine-Induced Current in Perfused Rat Myoballs

RICHARD HORN and MALCOLM S. BRODWICK

From the Department of Physiology and Biophysics, University of Texas Medical Branch, Galveston, Texas 77550. Dr. Horn's present address is Department of Physiology, Yale University School of Medicine, New Haven, Connecticut 06510.

ABSTRACT Spherical "myoballs" were grown under tissue culture conditions from striated muscle of neonatal rat thighs. The myoballs were examined electrophysiologically with a suction pipette which was used to pass current and perfuse internally. A microelectrode was used to record membrane potential. Experiments were performed with approximately symmetrical (intracellular and extracellular) sodium aspartate solutions. The resting potential, acetylcholine (ACh) reversal potential, and sodium channel reversal potential were all ~0 mV. ACh-induced currents were examined by use of both voltage jumps and voltage ramps in the presence of iontophoretically applied agonist. The voltage-jump relaxations had a single exponential time-course. The time constant, τ, was exponentially related to membrane potential, increasing e-fold for 81 mV hyperpolarization. The equilibrium current-voltage relationship was also approximately exponential, from −120 to + 81 mV, increasing e-fold for 104 mV hyperpolarization. The data are consistent with a first-order gating process in which the channel opening rate constant is slightly voltage dependent. The instantaneous current-voltage relationship was sublinear in the hyperpolarizing direction. Several models are discussed which can account for the nonlinearity. Evidence is presented that the "selectivity filter" for the ACh channel is located near the intracellular membrane surface.

INTRODUCTION

Acetylcholine (ACh) acts on the endplate of striated muscle by opening a large, water-filled pore which is selectively permeable to cations (Maeno et al., 1977; Huang et al., 1978; Dwyer et al., 1979). Attempts to understand the details of permeation have been hampered by the inability to control or even determine the ionic composition of the intracellular milieu. For example, measurement of ACh currents at very depolarized potentials is made difficult by the presence of large voltage-activated K currents. The K channel cannot be blocked simply with extracellular tetraethylammonium (TEA) because TEA also interacts strongly with the ACh channel (Adler et al., 1979). If the intracellular K could be replaced by a cation which is impermeable through the K channel, this difficulty would be alleviated. Another difficulty that is encountered in traditional studies of the motor endplate is the inability to test

J. GEN. PHYSIOL. © The Rockefeller University Press · 0022-1295/80/03/0297/25 $1.00 297
Volume 75 March 1980 297–321

quantitative theories of ion permeation. For example, ion permeation through the ACh channel may be depicted as the movement across two Eyring-type energy barriers with a low energy site (well) between them (Adams, 1979; Lewis and Stevens, 1979; Marchais and Marty, 1979). However, the details of the inner barrier must remain obscure until permeation is studied during systematic variations of the intracellular ionic composition.

We have developed a method for internal perfusion of muscle by using a suction pipette (Lee et al., 1978) on spherical myoballs (Fischbach and Lass, 1978) grown from cultured rat myotubes. We have employed a voltage clamp using a separate microelectrode to record membrane potential while passing current through the suction pipette. The use of the microelectrode reduces series resistance artifacts. In the experiments reported here we have examined ACh-induced currents in approximately symmetrical Na aspartate solutions using both voltage jumps and voltage ramps. A preliminary report has appeared (Horn et al., 1979).

MATERIALS AND METHODS

Tissue Preparation

The thigh muscles were removed from 1–3-d-old Sprague-Dawley white rats. The tissue was minced with scalpels, then dissociated at room temperature in a spinner flask containing 0.025 percent trypsin in divalent-free minimal attachment medium (Klebe, 1974). The supernate was removed at 15–20-min intervals and replaced with fresh trypsin solution until the tissue was completely dissociated. The cells were then centrifuged for 10 min at 3,000 rpm, resuspended in DV-10 (Dulbecco's medium enriched with 10% fetal calf serum, 1 mM proline, 0.5% chick embryo extract, 600 mg% glucose, 100 U/liter penicillin and 100 μg/ml streptomycin), and plated at a density of 1–4 × 10^6 cells per 60-mm Lux plastic tissue culture dish. The plates were then incubated at 37°C in 10% CO_2.

After 2–3 d myoblasts began fusing to form multinucleate myotubes. At this time, most of the plates were treated with 10^{-5} M araC (cytosine arabinoside, Sigma Chemical Co., St. Louis, Mo.) for 2 d to prevent further growth of fibroblasts. The araC had no apparent effect on the electrophysiological properties of the tissue.

In some plates, spherical myoballs formed spontaneously from myotubes. These were occasionally used in experiments, but usually the myotubes were treated for 1–3 d with 10^{-8} M vinblastine (Velban, Eli Lilly & Co., Indianapolis, Ind.) which induced myoball formation (Sachs and Lecar, 1977). The myoballs used for experiments were typically 70–120 μm in diameter. Both myotubes and myoballs twitched spontaneously in DV-10.

Solutions

The external solution was ½ Na Ringer containing 85 mM Na aspartate, 150 mM sucrose, 5 mM HEPES buffer, 1.5 mM $CaCl_2$, pH adjusted to 7.4 with NaOH. The internal solution was ½ Na SIS (standard internal solution) which consisted of 85 mM Na aspartate, 155 mM sucrose, 5 mM HEPES, 2 mM EGTA, 1 mM NaCl, pH 7.3. The activity of Na in each of these solutions was 63 ± 2 mM, as determined by a glass Na electrode (MI − 420, Microelectrodes, Inc., Londonderry, N. H.). A free Ca concentration of 1.47 mM in ½ Na Ringer was calculated from the critical stability constants for aspartate (Martell and Smith, 1974). In a few experiments 10^{-6} M

tetrodotoxin and 0.2 mM $CdCl_2$ were added to ½ Na Ringer in order to block currents in the voltage-activated Na and Ca channels, respectively. However, the Na channel block was incomplete, and all the experiments shown below did not make use of these blocking agents.

Voltage Clamp

Due to a significant series resistance in the tip of the suction pipette (see below), the transmembrane potential was assumed to correspond to the potential of the microelectrode (V_m, Fig. 1) with respect to circuit ground. Therefore, the voltage clamp circuitry was designed to clamp the microelectrode potential. The amplitude of the

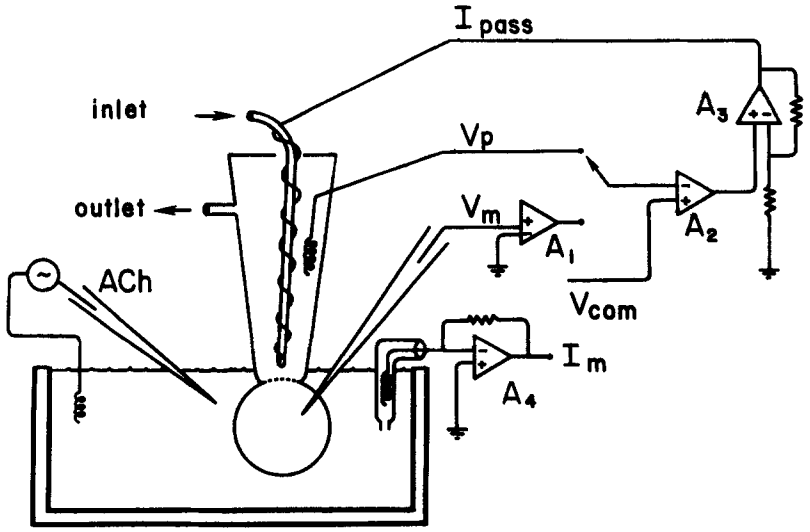

FIGURE 1. Experimental setup. Diagram shows myoball attached to suction pipette. Internal solution entered the inlet continuously. The suction was applied at the outlet. The potential recorded in the pipette by a chlorided silver wire was V_p. V_m was the potential recorded by the microelectrode. Either V_p or V_m could be voltage-clamped to the command voltage V_{com}. Current was passed into the cell by means of a 75 μm Pt wire wrapped around the polyethylene perfusion tubing, and led from the bath by a current-voltage converter with a 1 MΩ feedback resistor. ACh was applied iontophoretically with another microelectrode. A_1, W-P Instruments, Inc., model 750 electrometer (New Haven, Conn.); A_2, Tektronix, Inc., AM 502 differential amplifier (Beaverton, Ore.); A_3, Tektronix AM 501 operational amplifier (gain = 10); A_4, LF 356 operational amplifier (National Semiconductor Corporation, Santa Clara, Calif.).

net transfer function of the myoball, electrodes, and voltage follower on the microelectrode had a zero frequency asymptote of −6 dB and simple poles at 10, 6×10^3, and 5×10^6 Hz. In order to clamp at frequencies on the order of 10^4 Hz, the clamping amplifiers were designed to achieve a gain of >60 dB at 10^4 Hz. The electrical arrangement is shown in Fig. 1. The rise time of the voltage in response to a step command was usually less than 300 μs. The current signal was filtered at 10^4 Hz to remove high frequency noise.

Data Analysis

Data were displayed either on a Nicolet 1090 digital oscilloscope or on a Nicolet 1170 signal averager (Nicolet Instrument Corp., Madison, Wis.). Data were then stored either on a Kennedy digital tape recorder (model 9700, Kennedy Co., Altadena, Calif.) or on an Omnigraphic 2000 X-Y plotter (Houston Instruments, Austin, Texas). For voltage jump experiments, the sampling rate was usually 100–200 μs/point. For voltage ramps, the data were sampled every millisecond. 12-bit resolution was used in all cases.

For voltage jump experiments, control traces in the absence of ACh were subtracted digitally from experimental traces in the presence of ACh by use of a PDP 11-70 computer and a program kindly provided by Dr. Douglas C. Eaton. Additional analysis was performed on a PDP 11-20 computer (Digital Equipment Corp., Marlboro, Mass.).

Experimental Procedure

The experiments were performed in the tissue culture dishes after replacing the DV-10 with ½ Na Ringer. The experiments reported here were done at reduced room temperature (18°C).

A myoball was selected and sucked onto the tip of a broken and polished glass pipette (Fig. 1). The method is a modification of the technique described by Kostyuk and Krishtal (1977) and Lee et al. (1978). The inner diameter of the glass tip was 10–20 μm and had a resistance in the usual experimental solutions of ~700 kΩ. When the myoball was sucked onto the tip of the pipette, the membrane usually ruptured within a few seconds, as evidenced by a sudden drop in pipette potential (V_p, Fig. 1) and a sudden decrease in resistance to a hyperpolarizing current pulse. Most cells exhibited anodal-break spikes at the end of the current pulse. The steady-state resistance, using this method, was 7–15 MΩ in a healthy cell. The cell was then impaled with a 5–25 MΩ microelectrode (3 M KCl) for recording membrane potential. The cell could then be voltage-clamped, using either the potential recorded by a chlorided silver wire in the pipette, V_p, or that recorded by the microelectrode, V_m (Fig. 1). Current was passed into the pipette from a 75 μm platinum wire, and was led from the bath with a 3 M KCl agar bridge through a chlorided silver wire to a current-to-voltage converter with a 1 MΩ feedback resistor. The tip of the suction pipette was continuously perfused with ½ Na SIS at a rate of ~1 ml/min.

Acetylcholine (ACh, Sigma Chemical Co.) was applied iontophoretically by a pipette placed within 100 μm of the membrane surface. The pipette contained ~3 M ACh. The backing current was usually < 20 nA.

After impaling a myoball and observing an ACh response, i.e., an increased conductance in response to iontophoretic application of ACh, the cell was usually allowed to dialyze for 15–20 min to permit the exchange of intracellular ions. During this period, the steady-state membrane resistance, V_m/I_m (see Fig. 1) increased from ~4 to ~5 MΩ (Table I), presumably due to both (*a*) an increased sealing resistance between the membrane and electrodes, and (*b*) a replacement of intracellular K for Na. After recording the resting potential with the microelectrode, the cell was voltage-clamped, using V_m as a measurement of membrane potential. The ACh reversal potential was determined. Then a series of voltage steps were applied both in the presence and in the absence of ACh from a holding potential of −40 mV. In some experiments, the command voltage was an ~200 mV, 1 Hz triangular wave.

RESULTS

The first part of this section describes and evaluates the voltage clamp and the internal perfusion. The remainder of the section describes voltage jump

and voltage ramp experiments. The purpose of these experiments was to examine the voltage dependence of both the gating and the permeation of the ACh channel in this preparation.

Evaluation of the Voltage Clamp

The ability to voltage-clamp the myoball membrane accurately is limited by several factors. We will discuss three of these factors individually. They are the shunt resistance, R_{sh}, the pipette resistance, R_p, and the series resistance, R_s.

The shunt resistance, R_{sh}, is the sealing resistance between the suction pipette and the membrane. A low value of R_{sh} decreases the total impedance of the combined pipette and myoball. It can degrade the voltage clamp in two ways. It increases the output current load on the clamping amplifiers, and it increases the relative series resistance error. The latter effect may be especially severe, because it limits the capacity to determine and control the membrane potential while passing current.

TABLE I

RESTING POTENTIAL, ACh REVERSAL POTENTIAL, Na CHANNEL REVERSAL POTENTIAL, AND MEMBRANE RESISTANCE OF MYOBALLS

	Mean ± SEM (number of observations)
Resting potential	−1.4 ± 1.4 mV (19)
ACh reversal potential	−0.1 ± 0.9 mV (25)
Na channel reversal potential	+3.5 ± 3.4 mV (2)
Membrane resistance	5.2 ± 0.4 MΩ (19)

Data were obtained 20 min after impalement with the microelectrode. The external solution was ½ Na Ringer, the internal was ½ Na SIS. Membrane resistance was the steady-state response, V_m, divided by the stimulating current, I_m, a 3 nA hyperpolarizing step.

We have only indirect evidence that R_{sh} is high. The steady-state leakage resistance in chick myoballs impaled by two microelectrodes is ~4 MΩ (Fischbach and Lass, 1978). In our experiments R_m was ~5 MΩ (Table I). A finite value of R_{sh} would decrease the apparent value of R_m. Without having done the comparable experiment on rat myoballs, we can only suggest that R_{sh} is much greater than 5 MΩ. In any case our measured value of R_m is at least two orders of magnitude greater than R_s (see below).

The pipette resistance, R_p, can be determined by a comparison of the microelectrode voltage, V_m, with the suction pipette voltage, V_p, while passing current (see Fig. 1). A current step produced a larger voltage response in the suction pipette than the voltage response in microelectrode. This is illustrated in Fig. 2 A. The upper trace shows the V_m and the lower trace shows the V_p response to a 6 nA hyperpolarizing current step. The steady-state response was ~1.4 times larger in the suction pipette. In seven experiments V_p was 1.6 ± 0.3 (SD) times as large as V_m in response to a 3 nA current step. A difference

between V_m and V_p was not reported in similar experiments using snail neurons (Lee et al., 1978). In the remainder of this paper the membrane resistance, R_m, was measured from the steady-state change of V_m in response to a 3 nA hyperpolarizing current step. The difference between V_m and V_p is due to the pipette resistance, R_p, which is in series with the membrane

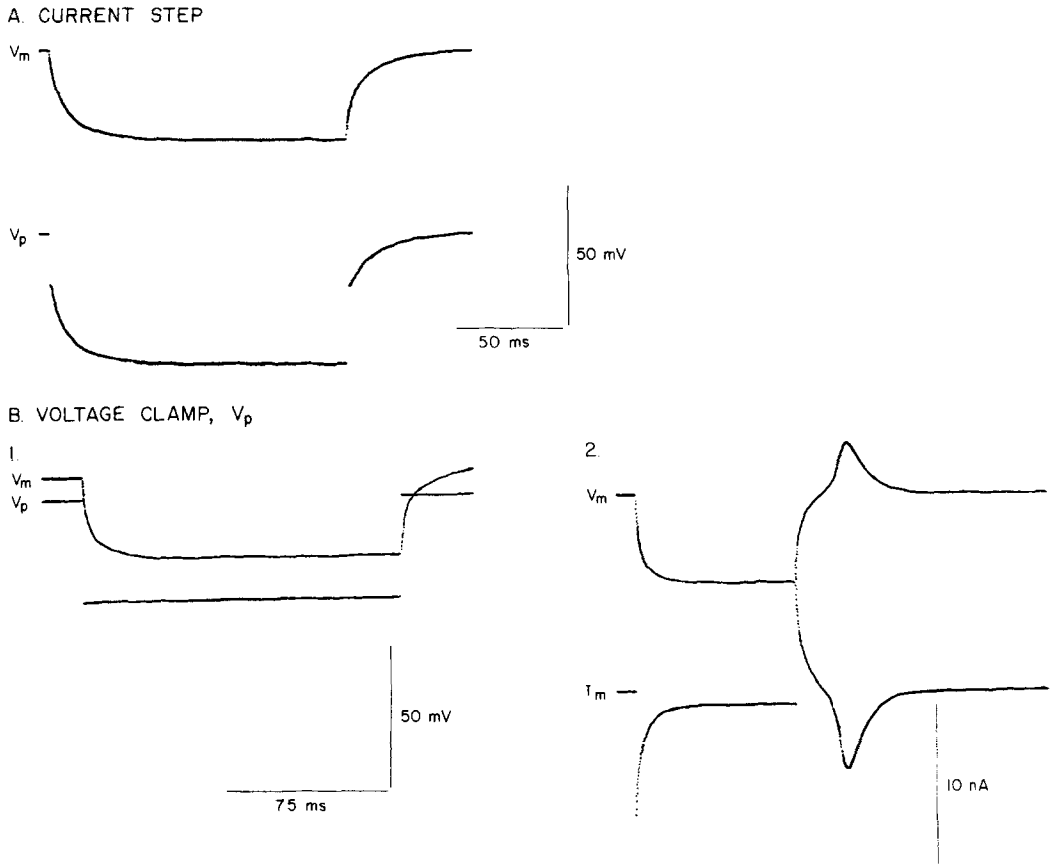

FIGURE 2. Comparison of V_m and V_p. (A) The voltage response of V_m and V_p in response to a 6 nA hyperpolarizing current step. The voltage, V_p, recorded in the suction pipette was larger. (B) The effect on V_m and I_m of voltage-clamping V_p. B1 shows that V_m charged with a time constant of 3.9 ms for a voltage step of V_p. B2 shows that, during anodal break inward current, a small action potential was recorded by the microelectrode, although V_p was constant (not shown).

resistance. This resistance was usually ~3 MΩ, which is larger than the ~700 kΩ resistance of the suction pipette in the bath. Apparently the tip of the pipette becomes partly occluded by cytoplasmic material or the myoball membrane.

The pipette and cell membrane may be represented as R_p in series with the

parallel R_m and C_m of the membrane. If V_p is voltage-clamped, a command voltage step, V_c, will produce an exponential response in V_m.

$$V_m = A \cdot V_c \cdot (1 - e^{-t/\tau})$$
$$A = R_m/(R_m + R_p) \qquad \tau = A \cdot R_p \cdot C_m \tag{1}$$

The values R_m, R_p, and C_m can be determined in the current injection mode by the response of V_m and V_p to a hyperpolarizing current step. These values then can be used to predict the time constant τ during the voltage clamp of V_p.

The voltage response (V_m) to a hyperpolarizing step of current was a single exponential charging curve. This is in contrast with results obtained from adult rat skeletal muscle where two passive time constants were observed (Duval and Léoty, 1978). However, Ritchie and Fambrough (1975) also observed a single time constant in rat myotubes. We estimated the area specific capacitance in three myoballs by dividing the measured capacitance by an apparent area (assuming that two-thirds of the spherical membrane area was intact after sucking up the cell onto the suction pipette). The average value was 13.6 $\mu F/cm^2$. Because of potentially large errors in estimating surface area, this value may be in error by as much as 50%. Nevertheless, it suggests that membrane infolding occurs, but without an extensive, narrow, T tubule system (Falk and Fatt, 1964). A preliminary electron microscope examination of rat myoballs showed this to be the case.[1]

Fig. 2 B shows the effect of voltage-clamping V_p in a myoball. In this cell $R_m = 4.1$ MΩ, $R_p = 1.24$ MΩ, and $C_m = 3.4$ nF. The predicted value of τ (see above) is then 3.2 ms. V_p closely approximated the command pulse, V_c, and produced an exponential response of V_m (Fig. 2 B1). The measured time constant was 3.9 ms, which is in reasonable agreement with the predicted value. It is clear that V_p is a poor representation of V_m, both in its absolute magnitude and in its time-course.

The insufficiency of using V_p for voltage-clamping the membrane is especially apparent in Fig. 2 B2 from the same cell. The lower trace shows I_m (see Fig. 1). The holding potential (measured by the microelectrode) was −30 mV. V_p (not shown) was a 75 ms, 40 mV hyperpolarizing voltage pulse. The steady-state response of V_m during the pulse was 30 mV. At the end of the pulse the cell responded with an anodal break inward current. Although this current was not accompanied by a voltage response of V_p, the microelectrode recorded a small action potential. In the presence of ACh the membrane resistance decreased as much as 12-fold at hyperpolarizing potentials. Under these conditions $R_p > R_m$, and attempts to compensate electronically for R_p were unsuccessful. Therefore, the remaining experiments discussed in this paper employed a voltage clamp of the microelectrode potential, V_m.

Fig. 3 shows another experiment in which the microelectrode potential, V_m, was voltage-clamped. V_0 is the holding potential (−40 mV in all experiments), and V_1 is the potential to which V_m was pulsed. In Fig. 3, $V_1 = -120$ mV. The

[1] Krauhs, J., R. Horn, and M. Brodwick. Unpublished observation.

dotted line represents zero current. Fig. 3 A shows the voltage jump current in the absence of ACh. The measured membrane resistance for this voltage jump was 2.1 MΩ. Note the anodal break Na current at the end of the voltage jump. In the presence of ACh (Fig. 3 B), the negative holding current

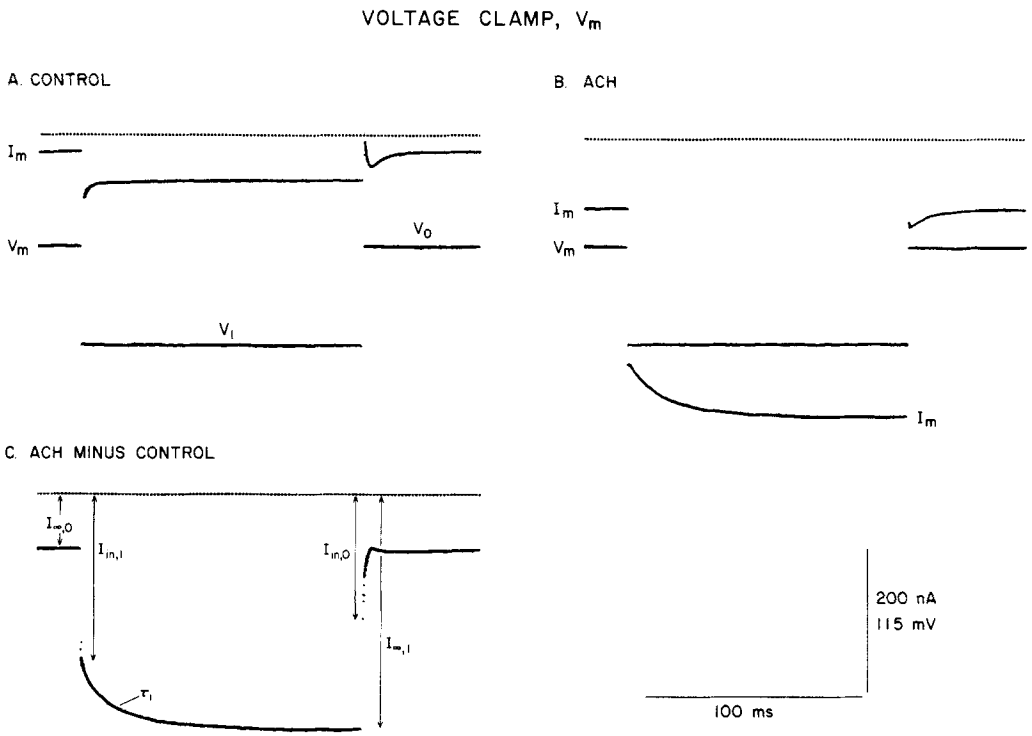

FIGURE 3. Voltage clamp of V_m and the effect of ACh. Holding potential, V_0, was −40 mV. In each record the dotted line represents zero current. Each record shows the effect of a 130 ms voltage jump to V_1, in this case, −120 mV. (A) The control response. Note the small anodal break inward current, during which V_m was constant. (B) The same voltage jump recorded in the presence of iontophoretically applied ACh. Note that the negative holding current increased in ACh and that the current relaxed to an equilibrium value after jumping to −120 mV. The magnitude and time-course of V_m was not affected by ACh, indicating that the gain of the clamping amplifiers was sufficiently high. (C) The effect of digitally subtracting I_m recorded in A from that recorded in B. $I_{\infty,0}$ is the ACh-induced current at V_0. $I_{in,1}$ is the instantaneous current induced at the beginning of the voltage jump. τ_1 is the relaxation time constant at V_1, in this case, 21.1 ms. The steady-state current at V_1 is $I_{\infty,1}$, and the instantaneous current at the end of the jump is $I_{in,o}$. Note that the current through the Na channel was not completely subtracted at the end of the jump (see text).

increased, and the voltage jump produced a large inward current. The steady-state resistance during this voltage jump was 276 kΩ. Both in the presence and in the absence of ACh, the rise time of V_m was ~300 μsec. Fig. 3 C shows

the result of digitally subtracting the control current from the current in the presence of ACh. The subtracted current represents the ACh-induced current. The capacity transient at the beginning of the voltage jump has been completely removed by the subtraction. Note, however, that the anodal break Na current was not subtracted. This is probably due to a series resistance error, as discussed below. The voltage jump current at V_1 was a single exponential with a time constant $\tau_1 = 21.1$ ms.

Evaluation of Series Resistance, R_s

The lumped membrane impedance is in series with both R_p and R_s. We used several criteria to estimate both the magnitude of R_s and its effect on ACh current. These criteria included (*a*) the voltage discontinuity in response to a current step, (*b*) the current capacity transient in response to a voltage step, (*c*) the difference in the current capacity transients in the presence or absence of ACh, (*d*) the time-course of the voltage jump relaxation, (*e*) the steepness of the τ vs. V_m relationship for voltage jump relaxations, and (*f*) the effect of current magnitude on the shape of the instantaneous current-voltage (*I-V*) relationship.

(*a*) In most experiments we did not observe a pronounced discontinuity of V_m in response to a step of current. This may be due to a finite capacitance to ground at the input of the voltage follower. This was usually not compensated.

(*b*) The current capacity transient in response to a voltage clamp step was usually both small in amplitude and so rapid that it could not be measured reliably. In many experiments the capacity transient occurred predominantly during the ~300-μs rise time of the voltage step. This sets an approximate upper limit for R_s of ~200 kΩ.

(*c*) A change in current capacity transient due to a reduction of R_m (e.g., in the presence of ACh), if measurable, could provide an estimate of R_s (see Eq. 1). However, even a large value of R_s, e.g., 200 kΩ, and a large change of R_m, e.g., by a factor of 10, leads to a <200 μs difference in the time constant. This could not be detected in our experiments. It was encouraging to note, however, that capacity transients were in all cases effectively subtracted, as seen in Fig. 3 C and especially in Fig. 5 A for a voltage jump to the reversal potential.

(*d*) The voltage jump relaxations were in all experiments well described by a single exponential, even at the most negative potentials where the amplitude of the relaxations were large (see Figs. 3 and 5). In Fig. 5A the voltage jump to −120 mV produced an ohmic jump, then a relaxation with a magnitude of 130 nA. Fig. 5 B shows that the current was well fitted with a single time constant. If R_s were as much as 200 kΩ, 130 nA would cause a 26 mV change in the actual membrane potential during the increasing current. From the normal voltage dependence of τ (see below), this would produce a nearly 10-ms difference in τ from the beginning to the end of the pulse. This was clearly not observed.

(*e*) A significant series resistance error would tend to decrease the apparent voltage dependence of τ. However, our τ vs. V_m relationship (see below) agrees well with published data on vertebrate endplate (for reference, see Steinbach and Stevens, 1976; Adams and Sakmann, 1978). A large R_s error would also

produce a deviation at negative potentials from the exponential relationship of τ and V_m. This was not observed.

(*f*) The instantaneous *I-V* relationship (below) was obtained with as much as four-fold differences in current magnitude in different experiments. However, the scaled instantaneous *I-V* curves superimposed (Fig. 7 A). We were able to discriminate ~10-mV shifts in these curves. From the relative current magnitudes we could set an upper limit of ~30 kΩ for R_s. In the worst cases this could produce an ~10 mV error in recorded voltage. This error would be most apparent at negative potentials because of the large driving force for the current and the increased channel lifetime (see below). The effects of such an error could produce shifts along the steady-state inactivation curve for the Na channel (Duval and Léoty, 1978). Such shifts could be responsible for the incomplete subtraction of anodal break Na currents (Figs. 3 and 5). However, such shifts would usually produce a <10% error in the conductance-voltage relationship of the ACh channel, and only at the most negative potentials.

Evaluation of the Internal Perfusion

Since the internal and external solutions were approximately symmetrical, we expected a 0 mV reversal potential for (*a*) the resting membrane, (*b*) the ACh-induced current, and (*c*) the Na channel current. The ACh reversal potential was determined directly within 1 mV (Fig. 4 *a*). Table I summarizes the results and suggests that the cells were adequately perfused. The possible effects of ion accumulation within the myoball during maximum ACh current were calculated from the apparent cell volume. The predicted changes in intracellular Na concentration during 30-s applications of ACh were <1 mM.

Voltage Jump Currents

For voltage jump experiments a 20–30-sec ACh pulse was delivered iontophoretically (Fig. 4 *b*). When the current reached a nearly steady-state level, four voltage jumps were given, usually in the following order: V_1 = −80, 0, +40, −120 mV. Fig. 5 shows typical voltage jump currents at these potentials. The jump to 0 mV shows only an off-relaxation at the holding potential. The jump to +40 mV produced an outward current with a rapid inward-directed relaxation. Because of the contamination of Na currents observed during the off-response with negative voltage jumps, the relaxations at −40 mV were determined during the off-response following positive voltage jumps. The off-relaxation time constants measured after jumps to 0 mV and to +40 mV always agreed within 5 percent. Fig. 5 B shows that the relaxations had exponential time-courses at all potentials.

Theory

The theoretical framework we have adopted has been formulated previously (Neher and Sakmann, 1975; Ascher et al., 1978). The "instantaneous" current immediately following a voltage jump to V_1 (Fig. 3 C) is given by

$$I_{in,1} = N\gamma_1 p_0 V_1, \quad (2)$$

where N is the total number of channels, γ_1 is the single channel conductance at V_1, and p_0 is the equilibrium probability of a channel being open at V_0. Because the reversal potential is close to 0 mV in all experiments, the driving force for the ACh current at potential V_1 is V_1. The steady-state current at V_1 is given by

$$I_{\infty,1} = N\gamma_1 p_1 V_1, \tag{3}$$

where p_1 is the equilibrium probability of a channel being open at V_1. The value for $I_{in,0}$ and $I_{\infty,0}$ have corresponding formulae.

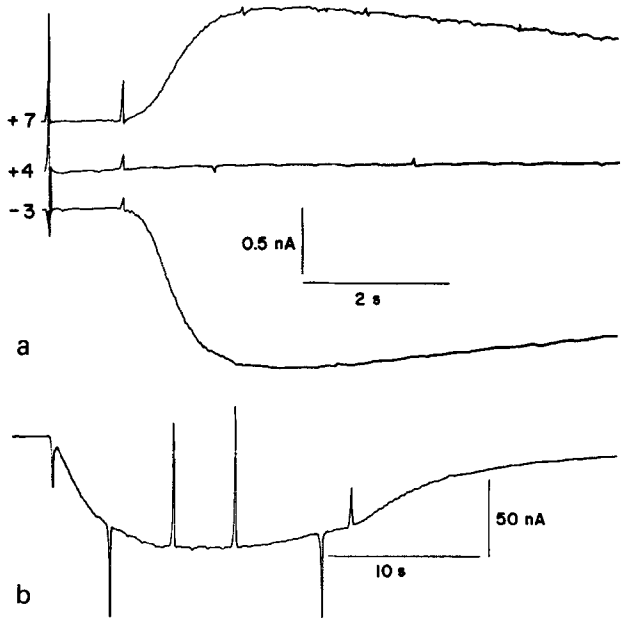

FIGURE 4. Effects of iontophoresis of ACh on I_m. (*a*) The effect of a 1 s application of ACh at three holding potentials, given on the left. The reversal potential in this cell was +4 mV. (*b*) The effect of a 20 s application of ACh. The beginning and end of application can be seen by stimulus artifacts. During the inward current response at $V_0 = -40$ mV, four voltage jumps were given, in the order $V_1 = -80$, 0, +40, and −120 mV. The magnitude of the voltage jump current responses shown is not an accurate representation of that recorded at higher sweep speeds on the oscilloscope.

For this analysis the ACh channel is assumed to exist in two states, closed and open, with the following rate constants:

$$\text{closed} \underset{\alpha}{\overset{\beta^*}{\rightleftharpoons}} \text{open}.$$

β^* is a pseudo first-order rate contant which depends on ACh concentration and on the binding constants for ACh on the ACh receptor. When the voltage

is stepped from V_0 to V_1, the rate constants α and β^* change instantaneously, and the current relaxes exponentially to its equilibrium value with a time constant,

$$\tau_1 = (\alpha_1 + \beta_1^*)^{-1}.$$

The equilibrium probability of a channel being open at V_i is given by

$$p_i = \beta_i^* \tau_i \text{ for } i = 1, 2. \quad (4)$$

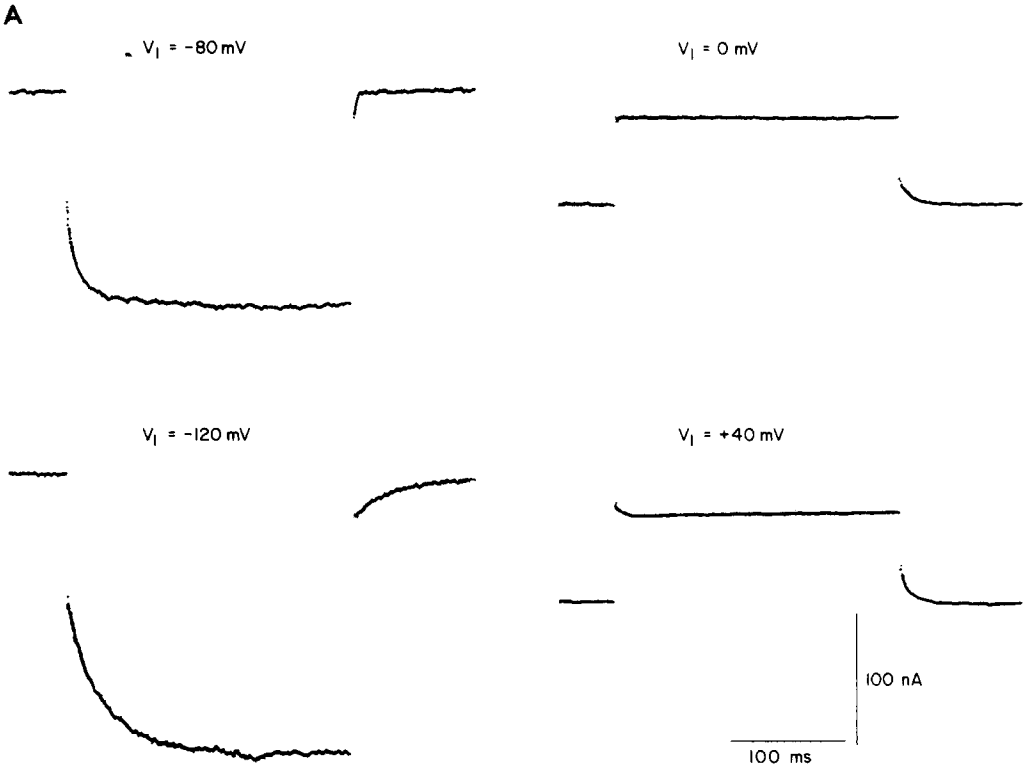

FIGURE 5. Voltage jump currents. (A) The voltage jump currents induced by ACh after subtracting control records. Notice that a step to 0 mV, the reversal potential, shows no observable relaxation. However, a comparison of the ohmic jumps before and after this jump gives evidence of a decrease in channel lifetime at 0 mV. The step to +40 mV shows an inward relaxation superimposed on the outward current. (B) Relaxations recorded in A are single exponentials. The relaxation at −40 mV was the off response after a jump to +40 mV.

α is an exponential function of voltage (Magleby and Stevens, 1972) with the form $\alpha\ (V) = a \exp\ (kV)$, where k is a constant representing the voltage sensitivity of α, and a is the closing rate constant at $V = 0$. In our experiments we used low iontophoretic doses of ACh in order to insure that β^* was negligible compared with α. This condition was checked in two ways. First,

the iontophoretic current was adjusted to a level that produced little desensitization (Fig. 4 *b*). Second, the relaxation time constants were determined at several iontophoretic current levels. An iontophoretic dosage was considered acceptable only if an increase of iontophoretic current by a factor of a third caused no change in τ at all potentials. Since $\beta_i^* \ll \alpha_i$, $1/\tau_i \approx \alpha_i$.

If β^* is voltage independent (Neher and Sakmann, 1975; Adams, 1977; Ascher et al., 1978), then the equilibrium (i.e., steady state) voltage depen-

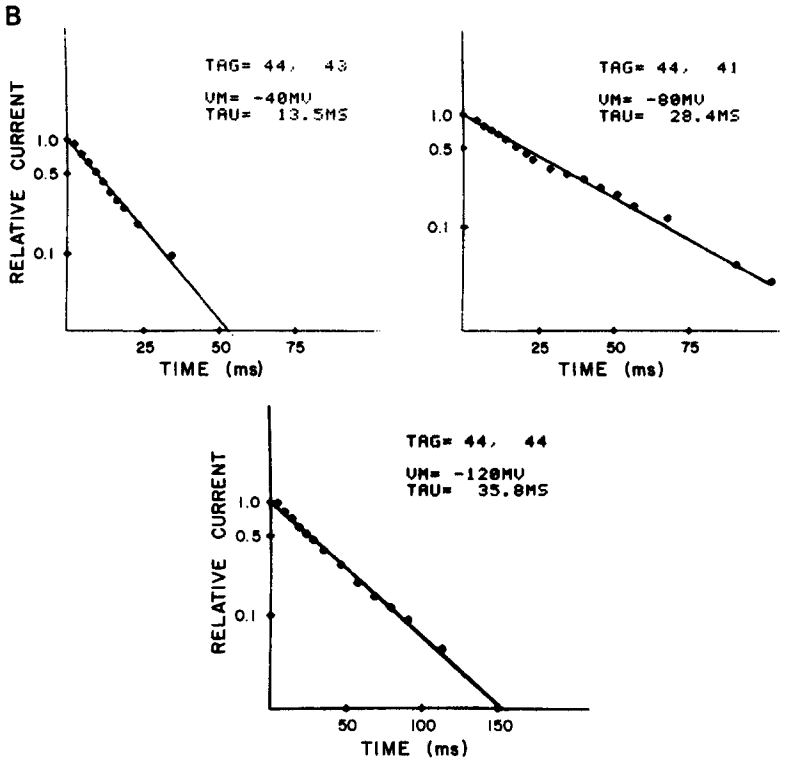

FIGURE 5

dence of ACh current will be the same as the voltage dependence of α, as implied by Eqs. 3 and 4. Note, however, that $I_{\infty,i}$ depends on N and γ_i. It was necessary to correct the voltage jumps currents for both of these factors to get a good estimate of p_i as a function of membrane potential (see below). The equilibrium current-voltage relationship was obtained using both voltage jumps and voltage ramps.

The relaxation time constants were usually determined by fitting single exponentials to the current relaxations. In some cases, however, the relaxations were difficult or impossible to measure. At positive potentials, for example, the relaxations were often too small in amplitude and too rapid to measure accurately. At the reversal potential the channel relaxation could not be

measured at all. However, it was still possible to estimate the relaxations at these potentials by comparing the relative amplitude of the instantaneous current jumps at the beginning and end of the voltage pulse (Neher and Sakmann, 1975; Ascher et al., 1978; Marchais and Marty, 1979). The ratio of jump amplitudes equals the ratio p_0/p_1, without the necessity of correcting for γ_i. If $\alpha_i \gg \beta_i^*$ and β_i^* is voltage independent, then

$$\alpha_1 = \alpha_0 p_0/p_1. \tag{5}$$

This method was used to estimate α_1 for $V_1 \geq 0$ mV.

Voltage Dependence of τ

The relationship between α and V_m was exponential from −120 mV to 0 mV (Fig. 6). The value of α decreased slightly from the exponential relationship at +40 mV. This may have been due to inaccuracies of measurement at this potential, or to a slight voltage dependence of β^*, since the calculated values of α at +40 mV assume β^* is voltage independent (Eq. 5). However, a similar trend in $\alpha(V)$ was observed at the endplate of *Rana temporaria* (Neher and

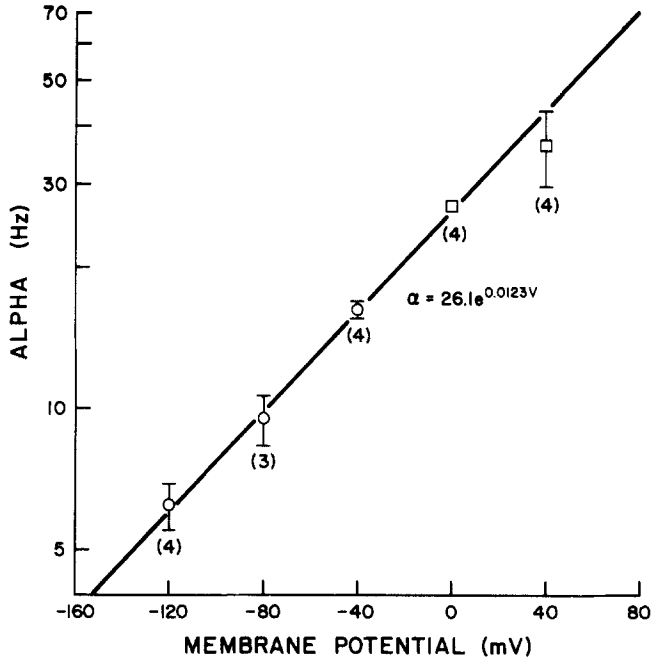

FIGURE 6. The relationship between alpha and membrane potential. α is plotted as frequency [$\alpha = (2\pi\tau)^{-1}$] on a logarithmic scale. The numbers in parentheses give the number of experiments. Each data point shows mean ± SEM. (○) Measured values (see Fig. 5 B). (□) Calculated values obtained by measuring the ratio of jump amplitudes before and after the voltage jump (see text). The straight line (drawn by eye) has the equation,

$$\alpha = 26.1 \exp (0.0123\ V_m)\ \text{Hz}.$$

Stevens, 1979). The assumption that $\alpha \gg \beta^*$ is given further support by the fact that the exponential relationship between α and V was maintained for the most negative potentials, where α was small. The voltage dependence of α ($1/k$ = 81 mV/e-fold change) is similar to values previously reported for other preparations (Steinbach and Stevens, 1976; Adams and Sakmann, 1978). The value of the preexponential factor a is smaller than that found at endplate (Steinbach and Stevens, 1976), but similar to values obtained with chick myoballs (Sachs and Lecar, 1977).

Instantaneous I-V

Fig. 4 *b* shows that the mean ACh-induced current at the holding potential was not the same during each voltage jump. The time-dependent changes in mean current were assumed to be due to changes in N, the number of available ACh channels. Thus, the magnitude of $I_{in,1}$ for each voltage step was scaled in a way that made N a constant. This was done by arbitrarily scaling the mean current at −40 mV to −90 nA for each voltage jump in each of four experiments. The value of $I_{in,1}$ was determined by extrapolating the exponentially relaxing current to the time of the change in voltage. For V_1 = 0 or +40 mV, $I_{in,1}$ was usually measured 400 μs after the beginning of the voltage jump. The pooled data for four experiments is shown in Fig. 7 *a*. At most potentials the standard error bars were smaller than the size of the symbol. The instantaneous *I-V* passed through the origin, as expected, and had a sublinear shape in the hyperpolarizing direction. The degree of sublinearity can be seen by comparing the chord conductance at −120 mV with that at −40 mV. The former was about 83% of the latter. The difference in chord conductance is indicative of a voltage dependence of the single-channel conductance. Sublinear I-Vs have been observed previously for both peak miniature endplate currents and single channel conductances (Dionne and Stevens, 1975; Gage and Van Helden, 1979).

A series resistance artifact could produce an apparent sublinearity from a linear instantaneous *I-V*. This is unlikely in our experiments, since the magnitude of such an error would increase with an increase in ACh current. However, the degree of sublinearity was similar in each of the four experiments, although the actual currents were as much as fourfold different.

The dotted line through the data points for the instantaneous *I-V* (Fig. 7*a*) was derived from a saturating, two-barrier, one-site model (see Discussion). In such a model the sublinearity is achieved by making the outer barrier asymmetrically located near the outer membrane surface.

Steady-State I-V

When corrected for N and γ_i at each potential, the steady-state *I-V* relationship provides an estimate of the equilibrium probability of a channel being open (see Eq. 3). $I_{\infty,1}$ was measured for each voltage jump in four experiments and corrected for N as above. The current value at each V_1 was corrected for γ_1 by multiplying it by γ_0/γ_1. The ratio γ_0/γ_1 was obtained from the instantaneous *I-V*. The resulting steady-state *I-V* is shown in Fig. 7 *b*. The chord conductance was an exponential function of voltage for negative potentials. The voltage

dependence in these four cells (k = 0.0094 mV^{-1}) is somewhat less than the voltage dependence of α (k = 0.0123 mV^{-1}).The aberrant data point at V = +40 mV may be due to an overestimate of γ_0/γ_1. Because of the rapidity of the relaxation at +40 mV, the instantaneous current may have been underestimated, which would lead to such an error.

The steady-state I-V can also be measured by using ramp clamps (Lester et al., 1975; Adams and Sakmann, 1978). Fig. 8 *a* shows the current in response to a 1 Hz triangular command voltage from −91 mV to + 81 mV. The control response to the triangular command voltage was nearly linear. When ACh was applied (note the arrow), both inward and outward current increased,

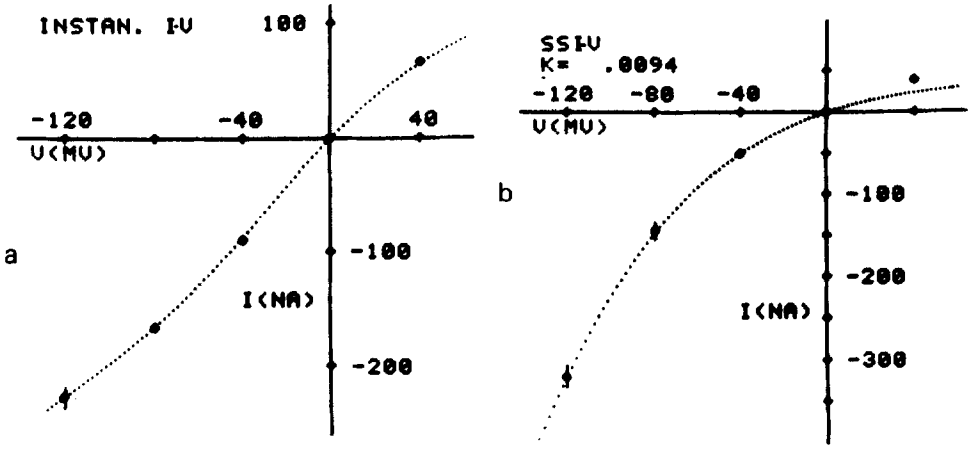

FIGURE 7. Instantaneous and steady-state I-V from voltage jumps. (*a*) The instantaneous I-V recorded for the step from V_0 to V_1. The steady-state current at −40 mV, $I_{\infty,0}$, was arbitrarily set at −90 nA for each voltage jump in four experiments and the currents, $I_{in,1}$, were scaled accordingly. The symbols show mean ± SEM for the four experiments. In most cases the standard error bars were smaller than the symbol. The dotted line is a theoretical fit of the data using the model and parameters shown in Fig. 9. (*b*) The steady-state I-V for the same experiments. In this case the mean current at V_0 was arbitrarily set at −50 nA. The currents were corrected for instantaneous rectification (see text). The dotted line is given by $I_{\infty,1} = C \cdot V_1 \cdot \exp(-k \cdot V_1)$, where $C = 8.58 \times 10^{-7}\ \Omega^{-1}$ and k = 0.0094 mV^{-1}.

although the inward rectification is obvious. 3 s after beginning ACh application, the current during a single hyperpolarizing ramp was analyzed in detail. After digitally subtracting the control current from the current recorded in the presence of ACh and correcting for the instantaneous I-V, the chord conductance was plotted against membrane potential on a semilogarithmic scale (Fig. 8*b*). The conductance was an exponential function of voltage for the entire voltage range, from −91 to +81 mV. The voltage dependence (k = 0.0098 mV^{-1}) was similar to the steady-state value obtained by voltage jumps in the same cell (k = 0.0097 mV^{-1}). In order to confirm that the conductance was at a steady-state level during the ramp clamp, we repeated

the experiment using 5-Hz triangular waves. The voltage dependence was identical to that observed for 1-Hz waves, indicating that the voltage change was sufficiently slow for the conductance to reach a steady state.

The voltage dependence of α was compared statistically with that of the steady-state *I-V* in order to determine if β^* had a significant voltage depen-

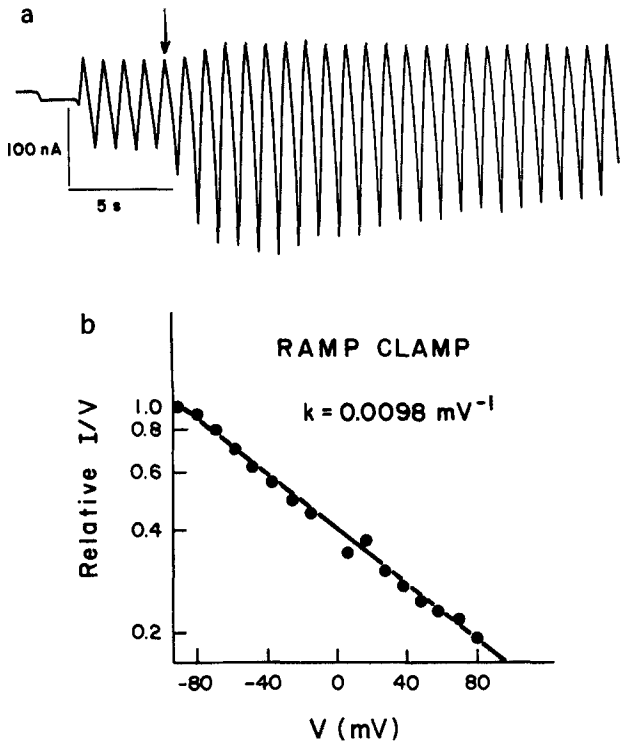

FIGURE 8. Ramp clamps. (*a*) The current response to a 1 Hz triangular command potential. The beginning of the trace shows zero current at +5.6 mV. The holding potential of −10 mV produced the negative shift of the current trace. Then the triangular wave drove the membrane potential from −91 to +81 mV. At the arrow ACh iontophoresis began. Notice the pronounced inward rectification induced by ACh. (*b*) The current-voltage relationship for a single hyperpolarizing ramp 3 s after beginning iontophoresis. The currents were corrected for leakage and instantaneous rectification. The equilibrium chord conductance was an exponential function of V_m, as shown, with a voltage dependence, $k = 0.0098\ mV^{-1}$.

dence. In six experiments the relationship between log α and voltage between −120 and −40 mV had a regression coefficient of $0.0122\ mV^{-1}$. The corrected steady-state *I-V* was determined in the same experiments by use of both voltage jumps and voltage ramps. Its regression coefficient was $0.00962\ mV^{-1}$. These values were found to be statistically different by use of Student's *t* test ($p < 0.001$; Steele and Torrie, 1960). Therefore β^* had a small (~390 mV/e-

fold change), but significant voltage sensitivity. This value is similar to that observed by Dionne and Stevens (1975).

These experiments support the notion that β^* has a slight voltage dependence, and extend previous observations to more positive potentials.

DISCUSSION

This paper presents the first study of ACh current in approximately symmetrical (external and internal) solutions. In general the data are consistent with results obtained under the usual asymmetric conditions, i.e., with Na as the predominant extracellular cation and K as the predominant intracellular cation. In particular, the voltage dependence of τ agrees well with previous reports (for references, see Steinbach and Stevens, 1976; Adams and Sakmann, 1978). The first part of Results deals with an evaluation of both the internal perfusion and the voltage clamp. The analysis can be summarized as follows: the adequacy of the internal perfusion was demonstrated by showing that the reversal potentials for (*a*) the resting membrane, (*b*) the ACh channel, and (*c*) the *Na* channel were all approximately 0 mV (Table I). The voltage clamp was considered to be adequate for the study of ACh current. The use of a microelectrode for recording membrane potential reduced the total series resistance from ~3 MΩ to <30 kΩ. For the largest currents this could produce ~10-mV errors in recorded voltage, which might cause, at most, 10% errors in the *I-V* relationship at very negative potentials. The voltage dependence of the ACh conductance could be underestimated by such an error. For potentials < -100 mV, in the worst cases the measured value of voltage dependence (k) would be about 90% of the actual value. In practice, however, there was no deviation of the value of k at negative potentials (see Fig. 6). The series resistance error, however, could cause significant effects on the Na channel conductance, which has a greater voltage dependence than that of the ACh conductance (Duval and Léoty, 1978).

Voltage-Dependent Gating

Since we were careful to use sufficiently low iontophoretic doses of ACh (see above), the $1/\tau$ vs. V_m relationship was equivalent to the α vs. V_m relationship. As in other endplate preparations, this was exponential over a range from -120 mV to 0 mV (Fig. 6). A slight deviation from exponentiality was already noted at +40 mV.

Since the voltage dependence of the equilibrium (i.e., steady state) *I-V* was similar to that of α (Figs. 6–8), the two-state model suggests that the channel-opening rate constant, β^*, has only a small voltage sensitivity (Eq. 4). This confirms previous results (Neher and Sakmann, 1975; Adams, 1977; Ascher et al., 1978; Marchais and Marty, 1979). However, there was a consistent deviation between the voltage dependence of τ and that of the corrected steady-state *I-V* . The steady-state *I-V* had a mean voltage dependence of 0.00962 mV^{-1} in six experiments using either voltage jumps or ramps. This value is significantly less than $k = 0.0122$ mV^{-1} obtained for the τ vs. V_m relationship in the same cells. The discrepancy was corrected by assuming a slight voltage sensitivity for β^*, ~390 mV/e-fold change. If the gating of the

ACh channel is accompanied by a change in effective dipole moment (Magleby and Stevens, 1972; Neher and Stevens, 1979), the channel closing corresponds to a change of about 75 debye while the channel opening corresponds to a change of only about 16 debye. This small voltage sensitivity of β^* can explain the deviation in the α vs. V_m relationship at +40 mV (Fig. 6). The mean value of α at +40 mV was determined, by use of Eqs. 4 and 5, to be 36 Hz, which falls below the straight line extrapolated from more negative potentials. By including the estimated voltage dependence of β^* in the calculation, $\alpha(40)$ increases to 45 Hz which is close to the value of 43 Hz given by the straight line at +40 mV.

Although our equilibrium *I-V* was slightly less voltage dependent than α, Adams and Sakmann (1978) recently found apparently steeper than normal equilibrium *I-V* curves. Their results are probably attributed to their use of slope rather than chord conductance. Our analysis shows that the equilibrium chord conductance, $G(V)$, is described by

$$G(V) = Ce^{-kV}, \tag{6}$$

where C is a constant, and k represents the voltage dependence of $G(V)$. The slope conductance, S, is

$$S(V) = \frac{\partial I_{\infty,1}}{\partial V} = C \cdot (1 - kV)e^{-kV}, \tag{7}$$

which in general is not an exponential function of V. However, when kV is small,

$$S(V) \approx C \cdot e^{-2kV} \tag{8}$$

which has twice the voltage dependence of $G(V)$.

Another way of looking at the apparent discrepancy caused by use of slope conductance is by use of a correction factor, H. The steepness of the voltage dependence is obtained by examining relative conductances at different potentials. The relative slope conductance is

$$\frac{S(V)}{S(V + \Delta V)} = \frac{G(V)}{G(V + \Delta V)} \cdot H, \tag{9}$$

where $H = (1 - kV)/(1 - k(V + \Delta V))$ and ΔV is a positive increment of voltage. Since k is positive, $H > 1$ for $kV < 1$. Therefore, for most cases where $V < +100$ mV, the relative slope conductance is steeper than the relative chord conductance. A trivial simulation shows that the equilibrium *I-V* of Adams and Sakmann (1978) is consistent with their τ vs. V data without the necessity of invoking a voltage dependence of β^* or other *ad hoc* assumptions.

Instantaneous I-V

The instantaneous *I-V* (Fig. 7*a*) was arbitrarily fitted with a saturating, two-barrier, one-site model (Adams, 1979; Lewis and Stevens, 1979; Marchais and Marty, 1979). This is a particularly simple model which satisfactorily describes

our data; however, further elaboration may well be required by the results of future experiments. Although the data are not sufficient to determine all of the free parameters in such a model, certain general principles can be formulated. It is important to indicate initially however, that the instantaneous *I-V* is not consistent either with that predicted by a Goldman-Hodgkin-Katz model (for example, see Lewis, 1979) or that predicted by a long pore model with neutral sites (Barry et al., 1979). Both models predict a linear *I-V* in symmetrical solutions, whereas our *I-V* shows a definite curvature.

The lower part of Fig. 9 shows the kinetic model, which assumes that the rate constants for hopping over the barriers are exponential functions of both barrier height and fractional membrane potential. The site was arbitrarily

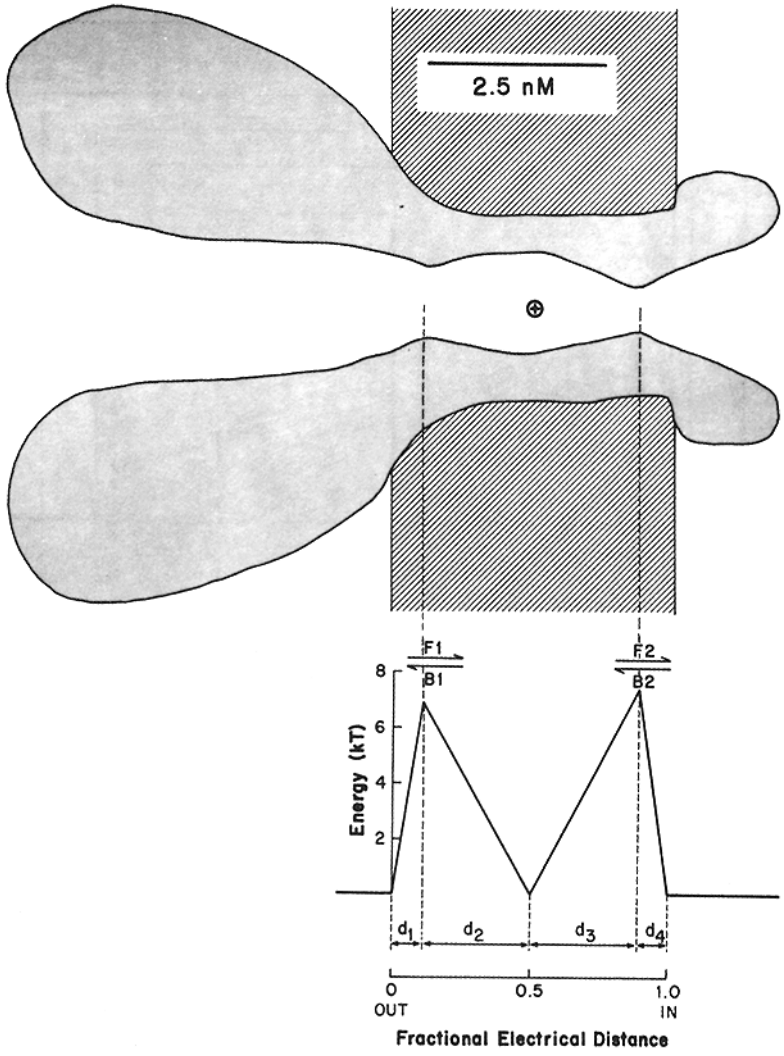

FIGURE 9

placed midway through the field. In accordance with Lewis and Stevens (1979) the energy level of the site was set at the solution level. If the barriers were symmetrically shaped and spaced (see Adams, 1979), the *I-V* would be slightly supralinear. The sublinearity in our model was produced by placing the peaks of the barriers asymmetrically close to the membrane surface. In the simulation used for Fig. 7 *a*, the peak of the outer (i.e., extracellular) barrier was placed 11% through the membrane field from the outer membrane surface. The sublinearity arises because negative potential cannot supply ions to the site as effectively as it drives them out of the site.

The sublinearity in the instantaneous *I-V* could be produced by other factors than the location of an outer barrier. For example, the Ca ions in the extracellular solution may not be negligible. In this case negative potentials could drive the Ca ions into the site, where they would reduce the apparent single channel conductance (Lewis, 1979; Lewis and Stevens, 1979). For example, if the dissociation constant for Ca ions at the mid-channel site is ~25 mM at −70 mV (Lewis, 1979), then the 1.5 mM Ca^{2+} we used in the bath could significantly saturate the site at −120 mV, where the dissociation constant would be ~3 mM for a simple first-order reaction. This would effectively reduce the "instantaneous" conductance at the more hyperpolarized potential. This simple model predicts that the instantaneous conductance at −120 mV will be 68% of that at −40 mV. We actually saw a reduction to only 83% of that at −40 mV. However, this simplistic scheme does not take into account a finite flux of Ca ions over the inner barrier. This Ca permea-

FIGURE 9. Two-barrier model. The upper part of the figure shows a hypothetical ACh receptor-channel complex (gray) in the lipid bilayer (cross-hatched). The outer dimensions are approximately drawn to scale from morphological evidence. A Na ion with the appropriate Stokes-Einstein radius is depicted in the site. The lower part of the figure shows the rate-limiting, free energy profile for ion movement through the channel. Free energy is plotted in kT units against fractional electrical distance of an applied membrane potential. The rate constants are

$$F1 = A \cdot \exp(-G_1) \cdot \exp(-d_1\, VF/RT)$$

$$B1 = B \cdot \exp(-G_1) \cdot \exp(d_2\, VF/RT)$$

$$F2 = B \cdot \exp(-G_2) \cdot \exp(-d_3\, VF/RT)$$

$$B2 = A \cdot \exp(-G_2) \cdot \exp(d_4\, VF/RT),$$

where G_1 and G_2 are the heights of the outer and inner barriers respectively, $A = 10^{11}\ s^{-1}\ mol^{-1}$, $B = 10^{13}\ s^{-1}$, V is applied membrane potential, and F, R, and T have their usual meanings. The fractional electrical distances shown are $d_1 = d_4 = 0.11$ and $d_2 = d_3 = 0.39$. The net flux through the channel is given by

$$J = \frac{C \cdot (B1 \cdot B2 - F1 \cdot F2)}{C \cdot (B2 + F1) + B1 + F2},$$

where C is the activity of Na ions. The single-channel current is given by $I = e \cdot J$, where e is the absolute value of the charge of an electron in coulombs.

bility will increase the dissociation constant, depending on the relative barrier heights. Therefore our data are at least qualitatively consistent with a Ca blocking scheme. If Ca ions are responsible for the sublinearity in the instantaneous *I-V*, then the *I-V* should be sublinear only in the hyperpolarizing direction. Our data are not detailed enough to show this, but the instantaneous *I-V* recorded by Gage and Van Helden (1979) was approximately linear for outward currents and sublinear for inward currents, again consistent with a Ca blocking scheme.

Two other factors could produce the sublinearity. Both are related to the fact that the ionic strength of the solutions used in our experiments was lower than that of normal Ringer. The first possibility is that "diffusion polarization" causes ion depletion and/or accumulation near the mouth of the channel (Läuger, 1976). This increases the access resistance to the channel when the ionic strength is low. The second possibility is that multiple binding sites occur in the ACh channel. In some versions of multiple-site models, the shape of the *I-V* changes from supralinear to sublinear as the ionic strength is decreased (Hladky et al., 1979). These possibilities remain to be tested.

The instantaneous *I-V* was steeper in the negative than in the positive direction. This was achieved by making the inner barrier (G_2) larger than the outer barrier (G_1). Although G_2 is only about one half a kT unit (where, in this case, k is Boltzmann's constant and T is °K) larger than G_1, this causes a twofold difference in the rate constants over each barrier. An equivalent way to fit the *I-V* was to make the barrier heights equal but include an extracellular surface potential of about −16 mV.

The model presented in Fig. 9 makes several predictions which are consistent with previously published data (for review, see Steinbach and Stevens, 1976). It predicts that, in normal Na Ringer, the single channel conductance will be about 25 pS at −80 mV. At this potential the open channel transports about 10^7 ions/s. The probability of the site being occupied is about 8×10^{-4}. This value may be low because of the high values assumed for the attempt frequency for leaving the site. The accuracy and adequacy of the model is testable by systematic variations of ionic composition on both internal and external membrane surfaces.

The upper part of Fig. 9 is a schematic representation of a cross section through the ACh receptor-channel complex (gray) residing in the lipid bilayer (cross-hatched). The approximate external dimensions of the protein and its position in the membrane were determined by use of X-ray diffraction, negative staining transmission electron microscopy, and low angle neutron scattering of the ACh receptor from *Torpedo californica* (Ross et al., 1977; Klymkowsky and Stroud, 1979; Wise et al., 1979). The structure of the channel walls is not known. However, it is tempting to suppose that the 25Å depression observed in the center of the ACh receptor, when viewed from the external membrane surface, is the opening of the channel. There is suggestive evidence that the "selectivity filter" of the channel corresponds to the inner barrier (G_2) of our proposed kinetic model:

(*a*) The selectivity filter has minimum dimensions of ~ 6.5 × 6.5Å (Maeno et al., 1977; Huang et al., 1978; Dwyer et al., 1979).

(*b*) Quaternary anesthetics, when applied extracellularly, probably bind to an intrachannel site which is well within the membrane field (Neher and Steinbach, 1978).

(*c*) The anesthetic QX-314 is incapable of reaching the binding site from the intracellular membrane surface (Horn et al., 1979).

(*d*) The dimensions of QX-314, determined from a Cory-Pauling-Koltun model (~8.2 × 6.0 × 12.8Å), are sufficiently large that it is unlikely that it can fit through the selectivity filter.

(*e*) Lewis and Stevens (1979) used a two-barrier, one-site model to fit reversal potentials and single-channel conductances observed with systematic changes of extracellular ion concentrations. They could fit their data only when the inner barrier height was equal to or greater than the outer barrier height.

(*f*) Our instantaneous *I-V* was best fit by assuming that the inner barrier was greater than the outer barrier.

It seems likely to us that both permeant ions and QX-314 are affected by the barrier asymmetry. In the latter case the inner barrier is insurmountably high. Although the outer barrier is depicted in Fig. 9 as a constriction in the channel, an image force barrier (Parsegian, 1975) may be sufficient to create the proposed energy barrier to ion movement.

The relative mobility of alkali metal cations is similar in water and in the ACh channel (Dwyer et al., 1979; Gage and Van Helden, 1979). This suggests that these ions exist in a hydrated form within the channel. Accordingly, the schematic drawing in Fig. 9 shows a scaled representation of a hydrated Na ion in the center of the channel.

We are grateful to P. Adams, P. Chauvin, W. D. Dickey, M. Ifshin, R. Klebe, W. Law, K. Lee, F. Sigworth, C. Stevens, and J. Strong for advice and comments. Virginia Bonnefil provided technical assistance. Dr. Charles Stevens provided computer facilities for data analysis.
Supported by grants NS-13778, CA-19017, and NS-12961 from the National Institutes of Health.

Received for publication 31 October 1979.

REFERENCES

ADAMS, P. R. 1977. Relaxation experiments using bath-applied suberyldicholine. *J. Physiol. (Lond.).* **268:**271–289.

ADAMS, P. R. 1979. A completely symmetrical barrier model for endplate channels. *Biophys. J.* **25:**70a (Abstr.)

ADAMS, P. R., and B. SAKMANN. 1978. A comparison of current-voltage relations for full and partial agonists. *J. Physiol. (Lond.).* **283:**621–644.

ADLER, M., A. C. OLIVEIRA, E. X. ALBUQUERQUE, N. A. MANSOUR, and A. T. ELDEFRAWI. 1979. Reaction of tetraethylammonium with the open and closed conformations of the acetylcholine receptor ionic channel complex. *J. Gen. Physiol.* **74:**129–152.

ASCHER, P., A. MARTY, and T. O. NEILD. 1978. Life time and elementary conductance of the channels mediating the excitatory effects of acetylcholine in *Aplysia* neurons. *J. Physiol. (Lond.).* **278:**177–206.

BARRY, P. H., P. W. GAGE, and D. F. VAN HELDEN 1979. Cation permeation at the amphibian motor end-plate. *J. Membr. Biol.* **45:**245–276.

DIONNE, V. E., and C. F. STEVENS. 1975. Voltage dependence of agonist effectiveness at the frog neuromuscular junction: resolution of a paradox. *J. Physiol. (Lond.).* **251**:245–270.

DUVAL, A., AND C. LÉOTY. 1978. Ionic currents in mammalian fast skeletal muscle. *J. Physiol. (Lond.).* **278**:403–423.

DWYER, T. M., D. J. ADAMS, and B. HILLE. 1979. Ionic selectivity of end-plate channels. *Biophys. J.* **25**:67a (Abstr.)

FALK, G., and P. FATT. 1964. Linear electrical properties of striated muscle fibres observed with intracellular electrodes. *Proc. R. Soc. Lond. Biol. Sci.* **B160**:69–123.

FISCHBACH, G. D., and Y. LASS. 1978. Acetylcholine noise in cultured chick myoballs: a voltage clamp analysis. *J. Physiol. (Lond.).* **280**:515–526.

GAGE, P. W., and D. VAN HELDEN. 1979. Effects of permeant monovalent cations on end-plate channels. *J. Physiol. (Lond.).* **288**:509-528.

HLADKY, S. B., B. W. URBAN, and D. A. HAYDON. 1979. Ion movements in pores formed by gramicidin A. *In* Membrane Transport Processes. C. F. Stevens and R. W.Tsien, editors. Raven Press, New York. **3**:89–103.

HORN, R., M. S. BRODWICK, and W. D. DICKEY. 1979. Asymmetry in the acetylcholine channel. *Neurosci. Abstr.* **5**:481.

HUANG, L-Y. M., W. A. CATTERALL, and G. EHRENSTEIN. 1978. Selectivity of cations and nonelectrolytes for acetylcholine-activated channels in cultured muscle cells. *J. Gen. Physiol* **71**:397–410.

KLEBE, R. J. 1974. Isolation of a collagen-dependent cell attachment factor. *Nature (Lond.).* **250**:248–251.

KLYMKOWSKY, M. W., and R. M. STROUD. 1979. Immunospecific identification and three-dimensional structure of a membrane-bound acetylcholine receptor from *Torpedo californica*. *J. Mol. Biol.* **128**:319–334.

KOSTYUK, P. G., and O. A. KRISHTAL. 1977. Separation of sodium and calcium currents in the somatic membrane of mollusc neurones. *J. Physiol. (Lond.).* **270**:545–568.

LÄUGER, P. 1976. Diffusion-limited ion flow through pores. *Biochim. Biophys. Acta.* **455**:493–509.

LEE, K. S., N. AKAIKE, and A. M. BROWN. 1978. Properties of internally perfused, voltage-clamped, isolated nerve cell bodies. *J. Gen. Physiol.* **71**:489–507.

LESTER, H. A., J-P. CHANGEUX and R. E. SHERIDAN 1975. Conductance increases produced by bath application of cholinergic agonists to *Electrophorus* electroplaques. *J. Gen. Physiol.* **65**:797–816.

LEWIS, C. A. 1979. Ion-concentration dependence of the reversal potential and single channel conductance of ion channels at the frog neuromuscular junction. *J. Physiol. (Lond.).* **286**:417–445.

LEWIS, C. A., and C. F. STEVENS. 1979. Mechanism of ion permeation through channels in a postsynaptic membrane. *In* Membrane Transport Processes. C. F. Stevens and R. W. Tsien, editors. Raven Press, New York. **3**:133–151.

MAENO, T., C. EDWARDS, and M. ANRAKU. 1977. Permeability of the end-plate membrane activated by acetylcholine to some organic cations. *J. Neurobiol.* **8**:173–184.

MAGLEBY, K. L., and C. F. STEVENS. 1972. A quantitative description of end-plate currents. *J. Physiol. (Lond.).* **223**:173–197.

MARCHAIS, D., and A. MARTY. 1979. Interaction of permeant ions with channels activated by acetylcholine in *Aplysia* neurones. *J. Physiol. (Lond.).* **297**:9–45.

MARTELL, A. E., and R. M. SMITH. 1974. Critical Stability Constants. Plenum Press, New York 24.

NEHER, E., and B. SAKMANN. 1975. Voltage-dependence of drug-induced conductance in frog neuromuscular junction. *Proc. Natl. Acad. Sci. U.S.A.* **72**:2140–2144.

NEHER, E. and J. H. STEINBACH. 1978. Local anaesthetics transiently block currents through single acetylcholine-receptor channels. *J. Physiol. (Lond.).* **277**:153–176.

NEHER, E. and C. F. STEVENS. 1979. Voltage-driven conformational changes in intrinsic membrane proteins. *In* The Neurosciences Fourth Study Program, F. O. Schmitt, and F. G. Worden, editors. MIT Press, Cambridge, Mass. 623–629.

PARSEGIAN, V. A. 1975. Ion-membrane interactions as structural forces. *Ann. N.Y. Acad. Sci.* **264:** 161–174.

RITCHIE, A. K., and D. M. FAMBROUGH. 1975. Electrophysiological properties of the membrane and acetylcholine receptor in developing rat and chick myotubes. *J. Gen. Physiol.* **66:**327–355.

ROSS, M. J., M. W. KLYMKOWSKY, D. A. AGARD, and R. M. STROUD. 1977. Structural studies of a membrane-bound acetylcholine receptor from *Torpedo californica. J. Mol. Biol.* **116:**635–659.

SACHS, F. and H. LECAR. 1977. Acetylcholine-induced current fluctuations in tissue-cultured muscle cells under voltage clamp. *Biophys. J.* **17:**129–143.

STEEL, R. G. D., and J. H. TORRIE. 1960. Principles and Procedures of Statistics. McGraw-Hill Book Co., New York 1–481.

STEINBACH, J. H., and C. F. STEVENS. 1976. Neuromuscular transmission. *In* Frog Neurobiology, a Handbook. R. Llinás and W. Precht, editors. Springer Verlag-New York, Inc. 33–92.

WISE, D. S., A. KARLIN, and B. P. SCHOENBORN. 1979. An analysis by low angle neutron scattering of the structure of the acetylcholine receptor from *Torpedo californica* in detergent solution. *Biophys. J.* **28:**473–496.